Physics – Uspekhi **53** (7) 691 – 701 (2010)

PHYSICS OF OUR DAYS

PACS numbers: **98.54. – h**, 98.62.En, 98.70.Sa

Physical conditions in potential accelerators of ultra-high-energy cosmic rays: updated Hillas plot and radiation-loss constraints

K V Ptitsyna, S V Troitsky

DOI: 10.3367/UFNe.0180.201007c.0723

Contents

Abstract. We review basic constraints on the acceleration of ultra-high-energy (UHE) cosmic rays (CRs) in astrophysical sources, namely, the geometric (Hillas) criterion and the restrictions from radiation losses in different acceleration regimes. Using the latest available astrophysical data, we redraw the Hillas plot and find potential UHECR accelerators. For the acceleration in the central engines of active galactic nuclei, we constrain the maximal UHECR energy for a given black hole mass. Among active galaxies, only the most powerful ones, radio galaxies and blazars, are able to accelerate protons to UHE, although acceleration of heavier nuclei is possible in much more abundant lower-power Seyfert galaxies.

1. Introduction

The origin of ultra-high-energy (UHE; energy $\mathcal{E} \geqslant 10^{19}$ eV) cosmic rays (CRs) remains unknown despite decades of intense studies (see, e.g., Ref. [1] for a comprehensive review and Ref. [2] for a recent pedagogical introduction). Recent studies, notably the observation of the Greisen–Zatsepin–Kuzmin [3, 4] cutoff by the HiRes experiment [5], further supported by the results of the Pierre Auger observatory (PAO) [6], suggest that at least a large fraction of UHECRs is accelerated in cosmologically distant astrophysical sources. The birth of (scientific) UHECR astronomy, however, awaits our firm understanding of the energies and primary composition of the observed cosmic rays, as well as identification of at least one astrophysical object where these particles are accelerated.

Given experimental ambiguities, it is important to understand theoretically which astrophysical objects may serve as UHECR accelerators. It was realized long ago that UHECR sources should be distinguished objects with extreme physical conditions. One simple criterion is geometric in nature: a particle should not leave the accelerator before it gains the required energy. Presumably, the particle is accelerated by the electric field and confined by the magnetic field; then the geometrical criterion is expressed in terms of the particle Larmor radius, which should not exceed the linear size of the accelerator (see, e.g., Ref. [7]). In the context of UHECRs, this condition is recognized as the Hillas criterion [8] and is often presented graphically in terms of the Hillas plot, where the accelerator size R and the magnetic field B are plotted. We note that even quite recent reviews use either cut-and-pasted or slightly refurbished versions of the original 25-year-old plot. However, astrophysics has experienced enormous progress, if not a revolution, during this time. One of the aims of this study is to give an updated version of the Hillas plot with references to either measurements (whenever possible) or estimates of the magnetic fields and sizes of potential astrophysical accelerators. The most important update corresponds to a wide variety of active galaxies whose sizes and magnetic fields differ by many orders of magnitude from one object to another, and hence some of them may, although most may not, accelerate particles to UHE.

K V Ptitsyna Lomonosov Moscow State University
Vorob'evy gory, 119992 Moscow, Russian Federation
E-mail: ptitsyna@gmail.com
S V Troitsky Institute for Nuclear Research,
Russian Academy of Sciences,
prosp. 60-letiya Oktyabrya 7a, 117312 Moscow, Russian Federation
Tel. (7-499) 135 21 69. Fax (7-499) 135 22 68
E-mail: st@ms2.inr.ac.ru

Received 21 January 2010
Uspekhi Fizicheskikh Nauk **180** (7) 723 – 734 (2010)
DOI: 10.3367/UFNr.0180.201007c.0723
Translated by K V Ptitsyna and S V Troitsky;
edited by A M Semikhatov

Another restriction on cosmic-ray accelerators is posed by the radiation losses, which inevitably accompany the acceleration of a charged particle. The corresponding constraints were studied, in particular, in Refs [8–11]. The radiation losses depend on the particular field configuration, and the maximal achievable energy of a particle in the loss-limited regime depends on the acceleration mechanism. Restricting oneself to particular mechanisms or particular field configurations may lead to contradictory results (cf. Refs [10, 11]). In this work, we review the radiation-loss constraints in different cases; they further limit the acceptable region on the updated Hillas plot. One of possible applications of these general constraints is the study of active galaxies correlated with the Auger events [12].

It should always be kept in mind that even if both geometric and radiation constraints are satisfied, they do not yet guarantee particle acceleration to the corresponding energy. Each particular source should be discussed in the context of the acceleration mechanism operating there.

The rest of the paper is organized as follows. In Section 2, we review constraints on potential UHE accelerators, that is, the model-independent Hillas geometric constraint and limitations due to radiation losses for particular acceleration mechanisms. In Section 3, we use modern astrophysical data and redraw the Hillas plot supplemented by radiation-loss constraints. Our results are summarized and discussed in Section 4, and brief conclusions are given in Section 5. Appendix 6 contains derivations of some formulas.

2. General constraints from geometry and radiation

An accelerator of UHECR particles should satisfy the following criteria.

• *Geometry*: an accelerated particle should be kept inside the source while being accelerated.

• *Power*: the source should have the required amount of energy to transfer it to accelerated particles.

• *Radiation losses*: the energy lost by a particle to radiation in the accelerating field should not exceed the energy gain.

• *Interaction losses*: the energy lost by a particle in interactions with other particles should not exceed the energy gain.

• *Emissivity*: the total number (density) and power of sources should be able to provide the observed UHECR flux.

• *Accompanying radiation* of photons, neutrinos, and low-energy cosmic rays should not exceed the observed fluxes, either for a given source or for the diffuse background (in particular, the ensemble of sources should reproduce the observed cosmic-ray spectrum).[1]

Our primary concern in this paper is geometric and radiation-loss constraints (others are briefly quoted when relevant); both restrict the magnetic field and the size of the accelerator and can be graphically represented on the Hillas plot.

2.1 The Hillas criterion

The Larmor radius $R_{\rm L}$ of a particle does not exceed the accelerator size, otherwise the particle escapes the accelerator and cannot gain further energy. This Hillas criterion sets the limit

$$\mathcal{E} \leqslant \mathcal{E}_{\rm H} = qBR \tag{1}$$

for the energy $\mathcal{E}$ gained by a particle with charge q in the region of size R with the magnetic field B.

2.2 Radiation losses

While Eqn (1) is a necessary limit, more stringent ones may arise from the energy losses: the maximal energy $\mathcal{E}_{\rm loss}$ that a particle can acquire in an infinite-size accelerator is determined by the condition

$$\frac{{\rm d}\mathcal{E}^{(+)}}{{\rm d}t} = -\frac{{\rm d}\mathcal{E}^{(-)}}{{\rm d}t}\,, \tag{2}$$

where the energy gain rate in the effective electric field $E = \eta B$ is (in the system of units where $c = 1$, which we use throughout the paper)

$$\frac{{\rm d}\mathcal{E}^{(+)}}{{\rm d}t} = q\eta B\,. \tag{3}$$

While keeping it explicit in the equations, we set the efficiency coefficient η equal to unity in the figures to obtain conservative (optimistic) limits for a given magnetic field: the electric fields in astrophysical objects are much less studied observationally compared to the magnetic ones, but it is always expected that $E \ll B$. Depending on the particular conditions in the accelerator, the maximal energy $\mathcal{E}_{\rm max}$ of a particle is limited by either geometrical or energy-loss arguments:

$$\mathcal{E}_{\rm max} = \min\{\mathcal{E}_{\rm H},\, \mathcal{E}_{\rm loss}\}.$$

The general expression for total radiation losses for a particle with a velocity $\mathbf{v}$ moving in arbitrary electric $\mathbf{E}$ and magnetic $\mathbf{B}$ fields is given by (see, e.g., Ref. [14])

$$-\frac{{\rm d}\mathcal{E}^{(-)}}{{\rm d}t} = \frac{2}{3}\,\frac{q^4}{m^4}\,\mathcal{E}^2\Big[(\mathbf{E}+\mathbf{v}\times\mathbf{B})^2 - (\mathbf{E}\,\mathbf{v})^2\Big]\,, \tag{4}$$

where q and m are the particle charge and mass. Using relativistic equations of motion, we can conveniently rewrite Eqn (4) as [15]

$$-\frac{{\rm d}\mathcal{E}^{(-)}}{{\rm d}t} = \frac{2}{3}\,\frac{q^2}{m^2\,(1-v^2)}\Big[\mathbf{F}^2 - \big(\mathbf{F}\,\mathbf{v}\big)^2\Big]\,.$$

The force $\mathbf{F}$ acting on the particle is further decomposed as $\mathbf{F} = \mathbf{F}_{\parallel} + \mathbf{F}_{\perp}$, where we define the parallel $\mathbf{F}_{||}$ and perpendicular $\mathbf{F}_{\perp}$ components with respect to $\mathbf{v}$, and hence $\mathbf{F}_{\perp}\,\mathbf{v} = 0$. Then

$$-\frac{{\rm d}\mathcal{E}^{(-)}}{{\rm d}t} = \frac{2}{3}\,\frac{q^2}{m^2(1-v^2)}\Big[F_{\perp}^2 + F_{\parallel}^2(1-v^2)\Big]. \tag{5}$$

It is apparent that the second term (the so-called curvature radiation) is suppressed compared with the first one (synchrotron radiation) by an extra power of $(1-v^2)$ and can therefore be neglected in the ultrarelativistic regime unless the synchrotron term is zero or very small itself. The synchrotron losses are dominant for any generic field configuration; however, in the very special regime $\mathbf{v} \parallel \mathbf{E} \parallel \mathbf{B}$ they vanish, and the losses are then determined by the curvature radiation.

[1] We note that the spectrum of cosmic rays accelerated in a particular source may be very different from the spectrum observed on Earth (cf. Ref. [13]).

2.3 Different acceleration regimes

Depending on the acceleration scenario, we consider diffusive (stochastic) and inductive (one-shot, or direct) mechanisms (see, e.g., Ref. [8] for a general discussion of these two approaches to UHECR acceleration).

The prime examples of diffusive processes are the Fermi first-order [16] and second-order (e.g., shock [17]) acceleration. Other possibilities include interaction with a medium by crossing an interface of layers with different velocities [18], and even transformation of a particle into a different one [19]. A recent review and more references can be found in Ref. [20].

In inductive mechanisms, the particle is accelerated continuously by a large-scale electric field and then leaves the accelerator. Strong ordered fields on relatively large scales are required; example scenarios are given, e.g., in Refs [21–25]. For our purposes, it is convenient to separate the inductive–acceleration scenarios into two groups, depending on whether the configuration of the accelerating field corresponds to losses mainly due to synchrotron radiation (e.g., large-scale jets [21]) or curvature (neutron stars [22] and black holes [23–25]).

2.3.1 Diffusive acceleration. The losses in this regime are the most serious. This scenario cannot be realized in strongly ordered field configurations with $\mathbf{v}||\mathbf{E}||\mathbf{B}$; therefore, the losses are determined by the synchrotron limit,

$$-\frac{\mathrm{d}\mathcal{E}^{(-)}}{\mathrm{d}t}=\frac{2}{3}\frac{q^2}{R_{\mathrm{L}}^2}\left(\frac{\mathcal{E}}{m}\right)^4=\frac{2}{3}\frac{q^4}{m^4}\,\mathcal{E}^2B^2\,. \tag{6}$$

This regime has been studied in Ref. [11], where it was shown (see Appendix A.2) that the maximal energy is limited by

$$\mathcal{E}_{\mathrm{d}}\simeq\frac{3}{2}\frac{m^4}{q^4}\,B^{-2}R^{-1}\,. \tag{7}$$

Diffusive mechanisms are quite generic and may work in any realistic environment that can host, for instance, a shock wave. Equation (7) does not rely on a particular acceleration mechanism and gives a (hardly reachable) upper limit for the maximal energy.

2.3.2 One-shot acceleration with synchrotron-dominated losses. In this regime, the energy loss rate is given by Eqn (6) and, with Eqn (3), formula (2) results in the maximum energy

$$\mathcal{E}_{\mathrm{s}}=\sqrt{\frac{3}{2}}\,\frac{m^2}{q^{3/2}}\,B^{-1/2}\eta^{1/2}\,. \tag{8}$$

This acceleration mechanism requires ordered fields throughout the acceleration site; its practical realization for UHECRs may work in the jets of powerful active galaxies [21].

2.3.3 One-shot acceleration with curvature-dominated losses. The energy loss rate is determined by (see Appendix A.1)

$$-\frac{\mathrm{d}\mathcal{E}^{(-)}}{\mathrm{d}t}=\frac{2}{3}\frac{q^2}{r^2}\left(\frac{\mathcal{E}}{m}\right)^4, \tag{9}$$

where r is the curvature radius of field lines, which is supposed to be of the order of the accelerator size, and Eqn (2) results in the maximum energy

$$\mathcal{E}_{\mathrm{c}}=\left(\frac{3}{2}\right)^{1/4}\frac{m}{q^{1/4}}\,B^{1/4}R^{1/2}\eta^{1/4}\,. \tag{10}$$

This mechanism requires ordered fields of very specific configurations, which, however, may be present in the immediate vicinity of neutron stars and black holes [22–25].

2.4 Summary of results for the maximum energy

We summarize the expressions for the maximum energy $\mathcal{E}_{\max}$ (in the comoving frame) attainable by a nucleus with atomic number Z and mass A in an accelerator of size R filled with the magnetic field B, for different acceleration regimes:

$$\mathcal{E}_{\max}(B,R)=\begin{cases}\mathcal{E}_{\mathrm{H}}(B,R), & B\leqslant B_0(R),\\ \mathcal{E}_{\mathrm{loss}}(B,R), & B>B_0(R),\end{cases}$$

where

$$B_0(R)=3.16\times10^{-3}\ [\mathrm{G}]\ \frac{A^{4/3}}{Z^{5/3}}\left(\frac{R}{1\,\mathrm{kpc}}\right)^{-2/3},$$

is determined from Eqns (1) and (7), (8), or (10) by requiring $\mathcal{E}_{\mathrm{H}}(B,R)=\mathcal{E}_{\mathrm{loss}}(B,R)$; the Hillas constraint is

$$\mathcal{E}_{\mathrm{H}}(B,R)=9.25\times10^{23}\ [\mathrm{eV}]\ Z\left(\frac{R}{1\,\mathrm{kpc}}\right)\left(\frac{B}{1\,\mathrm{G}}\right),$$

and the radiation-loss constraints are

$$\begin{aligned}\mathcal{E}_{\mathrm{loss}}(B,R)&=\mathcal{E}_{\mathrm{d}}(B,R)\\&=2.91\times10^{16}\,[\mathrm{eV}]\ \frac{A^4}{Z^4}\left(\frac{R}{1\,\mathrm{kpc}}\right)^{-1}\left(\frac{B}{1\,\mathrm{G}}\right)^{-2}\end{aligned}$$

for diffusive acceleration,

$$\mathcal{E}_{\mathrm{loss}}(B,R)=\mathcal{E}_{\mathrm{s}}(B,R)=1.64\times10^{20}\,[\mathrm{eV}]\ \frac{A^2}{Z^{3/2}}\left(\frac{B}{1\,\mathrm{G}}\right)^{-1/2}$$

for inductive acceleration with synchrotron-dominated losses, and

$$\begin{aligned}\mathcal{E}_{\mathrm{loss}}(B,R)&=\mathcal{E}_{\mathrm{c}}(B,R)\\&=1.23\times10^{22}\,[\mathrm{eV}]\ \frac{A}{Z^{1/4}}\left(\frac{R}{1\,\mathrm{kpc}}\right)^{1/2}\left(\frac{B}{1\,\mathrm{G}}\right)^{1/4}\end{aligned}$$

for inductive acceleration with curvature-dominated losses. Applications to particular objects and graphical representations of the constraints are given in Section 4 (Figs 8–12 in particular).

We note that the critical value $B_0(R)$ at which $\mathcal{E}_{\mathrm{H}}(B,R)=\mathcal{E}_{\mathrm{loss}}(B,R)$ is the same for all three acceleration regimes: in this case, the Larmor radius R_{L} and the size of the accelerator R are equal; within our approximation, they also coincide with the curvature radius r of the field lines. Therefore, the diffusive acceleration regime merges with the one-shot acceleration because the particle interacts with the shock wave only once in this limit case; moreover, Eqns (6) and (9) coincide and the two regimes of inductive acceleration result in similar losses.

3. Magnetic fields in particular sources

A number of astrophysical sources have been proposed where acceleration of cosmic rays to the highest energies can occur (see, e.g., Refs [26, 27] for reviews and a summary). In this section, we review experimental information on their magnetic fields in order to put them in their proper places on the

Hillas plot. General methods of astrophysical magnetic-field studies are discussed, inter alia, in Refs [28, 29]; however, a much wider variety of them is used for studies of individual sources.

3.1 Neutron stars, pulsars, and magnetars

Neutron stars host the strongest known magnetic fields in the Universe. In particular, magnetars (including anomalous X-ray pulsars) may have kilometer-scale fields $B \gtrsim 10^{14}$ G, while normal neutron stars have $B \sim (10^{11} - 10^{12})$ G. Observational evidence for these high fields is discussed in Section 6.3 in Ref. [30]. We also note a direct (although not widely accepted) observational method to measure B in neutron stars: the observation of spectral lines giving evidence of resonant Compton scattering at the cyclotron frequency in high-field media (see Ref. [31] for normal neutron stars and Ref. [32] for anomalous X-ray pulsars).

3.2 Active galaxies

For the purposes of the present study, we use a simplified classification of active galaxies (see textbooks [33, 34] and, for a more detailed discussion, Ref. [35]). Clearly, there are many intermediate states and peculiar objects that do not fit this classification well; while they should be studied individually if suspected to be UHECR sources, their relevant parameters (sizes and magnetic fields) are expected to be interpolated between those of better classified active galaxies.

Seyfert galaxies: spiral galaxies with bright emission-line nuclei; radio-weak; they do not have large-scale relativistic jets and often exhibit starburst activity.

Radio galaxies: radio-loud elliptical galaxies with relativistic jets. According to Ref. [36], they are classified into two luminosity classes: FR I (less powerful; jets brighter towards the core; jets may be curved) and FR II (more powerful; straight jets brighter at the hot spots at their end points).

Blazars: (almost) point-like objects with a nonthermal spectrum; strongly variable; similar in total power to radio galaxies; may be associated with radio galaxies whose jets are pointed towards the observer. They may be divided into BL Lac type objects (relatively low power; no emission lines; possible counterparts of FR I radio galaxies) and optically violent variable quasars (extremely powerful; may have emission lines; possible counterparts of FR II).

Low-power active galaxies (Seyferts) are much more abundant than radio galaxies and blazars.

Possible acceleration sites in active galaxies include both the central engine (immediate vicinity of the black hole and the accretion disk) and extended structures (jets, lobes, hot spots, and jet knots). We discuss the black-hole environment and extended structures separately because of the very different conditions for particle acceleration. We note that the term 'active galactic nucleus' (AGN) is often used to describe a region much larger than just the black hole and its accretion disc, and often includes inner jets (or sometimes even larger structures), which we consider separately.

3.2.1 Supermassive black holes and their environment. Measurements of magnetic fields in the central regions of galaxies have been performed by means of the following methods (see Fig. 1 for particular results).

1. *Synchrotron self-absorption*. Under certain conditions, the low-energy cutoff in the spectrum of a compact source may be detected and its shape may be proved to correspond to the absorption of synchrotron photons on themselves. If this is the case, then the magnetic field strength may be determined by means of the Slysh formula [45] or its modifications. The method works best for strong radio sources with resolved nuclear components [41–44].

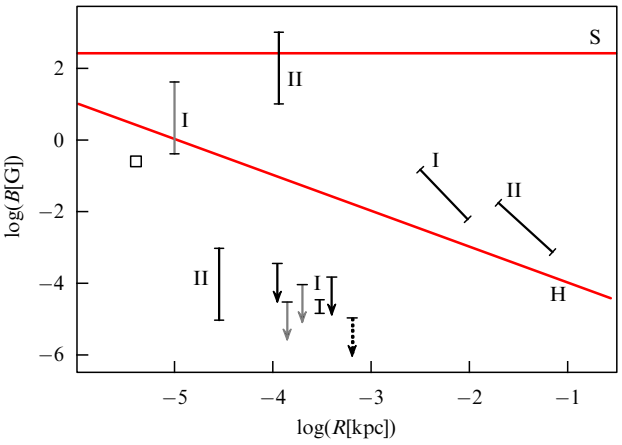

Figure 1. The size-field diagram for central regions of active galactic nuclei. Grey colors (square and arrows) correspond to Seyfert galaxies, error-bar lines marked I correspond to FRI radio galaxies, error-bar lines marked II correspond to FRII radio galaxies and quasars. Arrows: upper limits from the Zeeman splitting in megamasers (light grey, Ref. [37]; medium grey, Ref. [38]; dark grey, Ref. [39]). Dark (I) vertical error bar: Faraday rotation measurements, Ref. [40]. The grey box [41], light (I) vertical [42], dark (II) [43], and diagonal (I and II) [44] error bars correspond to the measurements by the synchrotron self-absorbtion method. The allowed region for acceleration of 10^{20} eV protons is located between thick red lines H and S (the lower line, H, corresponds to the Hillas limit; the upper one, S, corresponds to the radiation-loss limit for one-shot acceleration with synchrotron-dominated losses).

2. *Polarimetry*. Measurements of the Faraday rotation and of resulting depolarization give estimates of the magnetic field if the plasma density is known from independent observations [40].

3. *Zeeman effect in megamasers*. Megamasers are compact sources of coherent radiation in molecular clouds inside or around the accretion disk. The current precision allows putting very stringent constraints on the magnetic fields in these regions from nonobservation of the Zeeman splitting in megamasers in nearby Seyfert galaxies [37–39].

4. *The iron* K_α *line*. Measurements of the width and shape of this X-ray line may provide important information about circumnuclear dynamics; in particular, it can be used to estimate the magnetic field, although present constraints are quite weak [46]. But all these direct measurements cannot probe the most interesting region in the immediate vicinity of the central black hole, a few Schwarzschield radii (R_S) from the center. This region is particularly important because theoretically motivated configurations of electric and magnetic fields may allow the negligible synchrotron radiation of accelerated particles and thus for (relatively weak) curvature-dominated radiation losses. Our lack of understanding of the field structure in the accretion disk is transformed into uncertainties in the inferred magnetic fields B_{BH} at the black hole horizon (see, e.g., Ref. [47] for a summary of models used for this extrapolation). Direct estimates of B_{BH} are therefore not only scarce but also model dependent.

On the other hand, the parameters of the environment of a black hole, and in particular the value of B_{BH}, depend strongly on the black hole mass M_{BH}. A conservative upper

limit on $B_{\rm BH}$ follows from the condition that the maximal rate of extraction of the rotational energy of a black hole does not exceed the Eddington luminosity [48] (see Ref. [49] for a detailed discussion),

$$B_{\rm BH} \lesssim 3.2 \times 10^8 \left(\frac{M_{\rm BH}}{M_\odot}\right)^{-1/2} \text{G}. \quad (11)$$

Quite old but popular models estimate the $M_{\rm BH}$–$B_{\rm BH}$ relation from the pressure balance (radiation pressure equals the magnetic viscosity pressure) [50, 51]:

$$B_{\rm BH} \sim 10^8 \left(\frac{M_{\rm BH}}{M_\odot}\right)^{-1/2} \text{G}. \quad (12)$$

An efficient method to constrain the relation between $M_{\rm BH}$ and $B_{\rm BH}$ was found in Ref. [52] in the framework of a particular (not generally accepted) theoretical model in which both $M_{\rm BH}$ and $B_{\rm BH}$ are related to the observable luminosity at 5100 Å. This gives somewhat lower values of $B_{\rm BH}$ than Eqn (12); the best fit is

$$\log\left(\frac{B_{\rm BH}}{1\,\text{G}}\right) = (9.26 \pm 0.39) - (0.81 \pm 0.05) \log\left(\frac{M_{\rm BH}}{M_\odot}\right), \quad (13)$$

where we took the central values of the coefficients from Ref. [52] and estimated the error bars based on the data in that paper. In two cases where rather firm and model-independent values of $B_{\rm BH}$ can be inferred from the observations (synchrotron self-absorption measured at different radii down to 0.1 pc and extrapolated to $R_{\rm S}$, Ref. [44]), we estimated the corresponding $M_{\rm BH}$ and found that both values are in good agreement with Eqn (13), although the precision is quite low.

Estimates of $B_{\rm BH}$ versus $M_{\rm BH}$ are summarized in Fig. 2. We use the upper limit, Eqn (11), to estimate $B_{\rm BH}$ for a given $M_{\rm BH}$; we note, however, that realistic values of $B_{\rm BH}$ are 1–2 orders of magnitude lower. For curvature-dominated radiation losses, higher B always results in higher $\mathcal{E}_{\rm max}$, and hence this assumption is conservative for our purposes.

The size R of the potential acceleration region (that is, the region occupied by $\mathbf{E}\,||\,\mathbf{B}$ fields suitable for curvature-dominated losses) is of the order of $R_{\rm S}$; therefore, both R and B are governed by a single parameter $M_{\rm BH}$, and hence we can express the maximum energy through $M_{\rm BH}$ using the results in Section 2.4. Assuming that

$$R \sim 5R_{\rm S} \approx 5 \times 10^{-5} \frac{M_{\rm BH}}{10^8 M_\odot} \text{ pc}, \quad (14)$$

we find that for any reasonable $M_{\rm BH}$ (ranging from $\sim 10^6 M_\odot$ for normal galaxies through $(10^7 - 10^8) M_\odot$ for Seyfert galaxies to $(10^9 - 10^{10}) M_\odot$ for powerful radio galaxies and quasars), the maximum energy is determined by radiation losses rather than by the Hillas condition and is given by

$$\mathcal{E}_{\rm max} = \mathcal{E}_{\rm c} \simeq 3.7 \times 10^{19} \frac{A}{Z^{1/4}} \left(\frac{M_{\rm BH}}{10^8 M_\odot}\right)^{3/8} \text{eV}. \quad (15)$$

This general constraint is presented in Fig. 3 for different nuclei (A, Z); for comparison, results of numerical simulations of particle acceleration near a supermassive black hole [25] are also plotted.

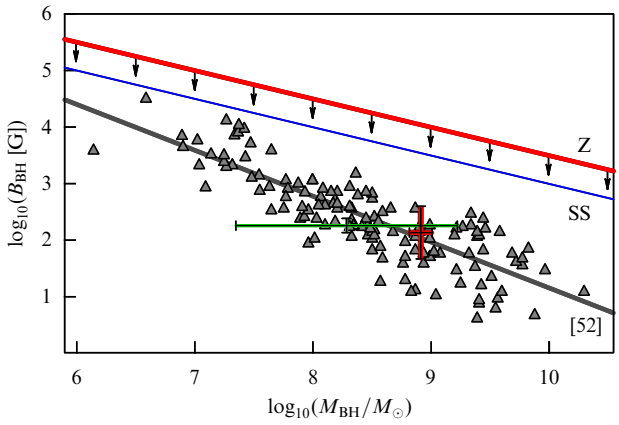

Figure 2. Magnetic field $B_{\rm BH}$ at the black hole horizon versus the black hole mass $M_{\rm BH}$. Triangles are estimates in Ref. [52] (determined in the framework of a particular, not generally accepted model) and the grey line (marked [52]) represents their best fit, Eqn (13). The two points with error bars correspond to experimental estimates of $B_{\rm BH}$ in Ref. [44], using the synchrotron self-absobtion method ($M_{\rm BH}$ estimated by us using the stellar velocity dispersion from HyperLEDA [53] (thick error bars, FRI radio galaxy 3C 465) and 2MASS K_s magnitude quoted in NED [54] (thin error bars, FRII radio galaxy 3C 111); see Ref. [54] for details). The thin line (SS) corresponds to the Shakura–Sunyaev estimate, Eqn (12). Thick line (Z) represents the Znajek upper limit, Eqn (11). The this conservative upper limit is used in our estimates of the maximal cosmic ray energy.

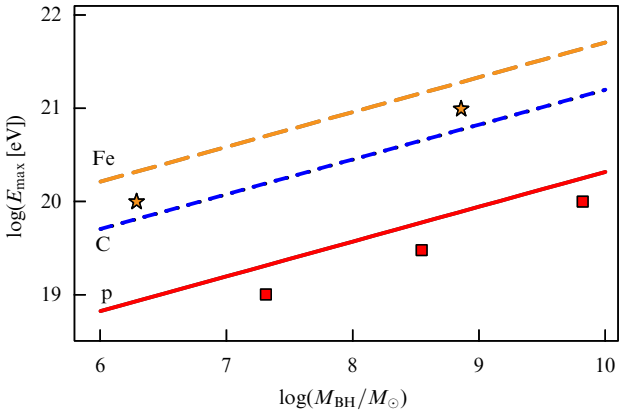

Figure 3. Upper limit on the maximal attainable energy of protons (solid line), carbon nuclei (dotted line), and iron nuclei (dashed line) for acceleration with curvature-dominated losses near a supermassive black hole, Eqn (15). The maximum energy obtained in numerical simulations in a particular mechanism [25] is shown by boxes (protons) and stars (iron nuclei); these data were obtained from Figs 5 and 10 in Ref. [25] and Eqn (11) in this paper.

In a way similar to other observational manifestations of supermassive black holes, the details of both cosmic ray acceleration and radiation losses may depend on the accretion rate, accretion mode, environment, and so on. However, we are interested here in the upper limit on the maximum attainable energy of a cosmic-ray particle, which is determined by $M_{\rm BH}$, as we have just demonstrated.

3.2.2 Jets and outflows of active galaxies. Active galactic nuclei fuel large-scale (from subparsec to megaparsec length) relatively extended linear jets. Revolutionary progress in the angular resolution of radio (sub-milliarcsecond) and X-ray (sub-arcsecond) imaging allowed detailed studies

and modeling of physical conditions in jets. We briefly review the basics of the current understanding of jet properties following Refs [55, 56].

Seyfert galaxies have extended structures, which are often noncollimated (with the opening angle 45° or more) and are nonrelativistic; they are sometimes referred to as 'outflows,' with the term 'jets' reserved to strongly collimated relativistic flows. X-ray emission from these outflows, when present, is well described by thermal radiation (sometimes associated with star-forming regions in the outflow [57]).

Relativistic jets reveal themselves in nonthermal X-ray emission that is now being studied in great detail. The jets are spatially resolved into components; in nearby jets (Cen A), the inner and outer layers and bright knots are resolved. It is often assumed that all jets are fueled by the central black hole; the energy flux is dominated by the magnetic field energy at sub-parsec scales but becomes particle-dominated at parsec scales. The emission of low-luminosity sources (FR I radio galaxies and BL Lacs) is adequately described by the synchrotron models in the range from the radio to the X-ray band; their jets are decelerated by the entrainment of gas and eventually dissipate. High-power FR II and quasar jets bring their energy flux directly to their terminal hot spots and require an additional (e.g., Compton) component to describe their spectra. Comparison of radio and X-ray observations gives rather firm evidence of the origin of the emission of FR I jets from accelerated particles and of the acceleration of these particles, not only in a finite number of shocks but also by means of some distributed mechanism along the jet [58, 59]. Quite rarely, relativistic jets are present in exceptionally powerful Seyfert galaxies; in these cases, they have properties very similar to FR I jets [56]. Models of multifrequency spectra allow constraining the magnetic field, the key parameter of synchrotron radiation. The estimates also depend on the electron density; degeneracy is often removed either by the equipartition assumption or by a simultaneous measurement of the self-Compton component, when applicable. When error bars are given, they include the corresponding uncertainties. Some of these estimates [56, 60–63] are presented in Fig. 4. In some cases, the existence of ordered fields in jets has been proved, and therefore inductive acceleration may be possible (see, e.g., Ref. [21]).

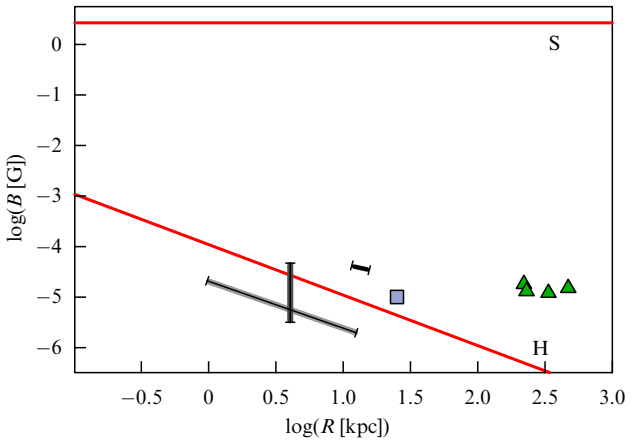

Figure 4. The size-field diagram for jets and outflows of individual active galaxies. Grey colors correspond to Seyfert galaxies, data from Refs [56] (light-grey diagonal line), [60] (grey vertical error bar), [61] (short dark grey diagonal). The blue box corresponds to an FR I radio galaxy [62]; green triangles represent quasar jets [63]. The allowed region for acceleration of 10^{20} eV protons is located between the thick red lines H and S (the lower line, H, corresponds to the Hillas limit; the upper, S, corresponds to the radiation-loss limit for inductive acceleration with synchrotron-dominated losses).

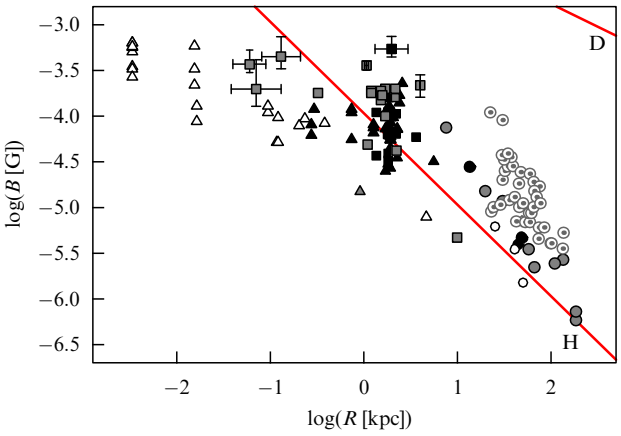

Figure 5. The size-field diagram for knots (triangles), hot spots (squares), and lobes (circles) of individual powerful active galaxies. Filled black symbols correspond to quasars and blazars, filled grey symbols correspond to FR II radio galaxies, empty symbols correspond to FR I radio galaxies (data from Ref. [66], X-ray observations assuming equipartition); squares with error bars represent the 'best-guess' estimates in Ref. [67]; dotted grey circles correspond to FR II lobes studied in Ref. [68] (comparison of radio and X-ray observations without the equipartition assumption). The allowed region for acceleration of 10^{20} eV protons is located between thick red lines H and D (the lower line, H, corresponds to the Hillas limit; the upper, D, corresponds to the radiation loss limit for diffusive acceleration).

3.2.3 Jet knots, hot spots, and lobes of powerful active galaxies. When a relativistic jet is present, it may be accompanied by internal shock regions (knots), terminal shock regions (hot spots), and extended regions in the intergalactic space fueled by the jet after its termination (lobes). These regions are typically absent in low-power active galaxies (Seyfert galaxies): knots are observed mostly in jets of FR I radio galaxies and quasars, lobes are typical for radio galaxies, and hot spots are present in the most powerful FR II radio galaxies and quasars. Magnetic fields can be determined either by X-ray synchrotron observations alone (assuming equipartition) or by combined multifrequency observations of both synchrotron and Compton radiation (allowing the relaxation of the equipartition assumption, which a posteriori turns out to be a good approximation; see, e.g., Ref. [64]).[2] A summary of the measurements in [66–68] is given in Fig. 5.

3.3 Star formation regions and starburst galaxies

Measurements of the magnetic field in galactic star-forming regions have become possible with the Zeeman splitting in masers in circumstellar disks [69–72] and infrared imaging polarimetry [73]. Although these regions in our Galaxy have never been considered as possible sites of UHECR acceleration, these measurements may give some hints about the fields in larger star-forming regions in starburst galaxies, where particles could be accelerated to very high energies, for example, in shocks from subsequent supernova bursts [74];

[2] An interesting approach to the determination of the magnetic field in a knot in M87 [65] exploits the energy dependence of the energy loss rate, assuming it is synchrotron dominated. The resulting field ~ 0.6 mG is in good agreement with equipartition-based estimates.

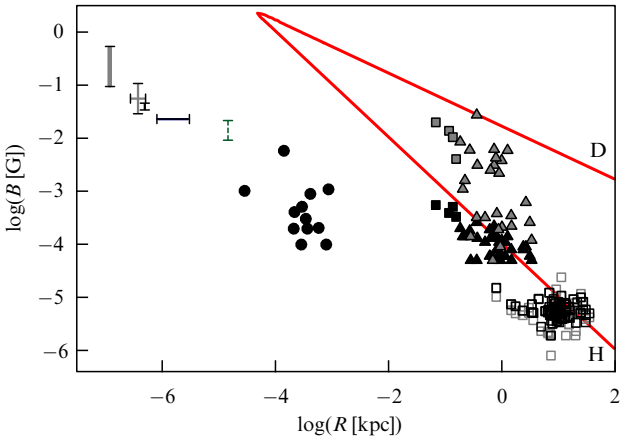

Figure 6. The size-field diagram for galactic star-forming regions ($R \gtrsim 1$ pc) and starburst galaxies ($R \gtrsim 0.1$ kpc). Thick (error-bar) lines correspond to measurements of the Zeeman splitting in masers (thick grey, Ref. [69]; short vertical, Ref. [70]; horizontal, Ref. [71]; dashed vertical, Ref. [72]). Black dots represent results of submillimeter imaging polarimetry of Ref. [73]. Data for normal (empty squares), starburst (triangles), and extreme starburst (filled squares) galaxies are taken from Ref. [75]; black symbols correspond to the minimal-energy field estimates while grey symbols correspond to equipartition field estimates. The allowed region for acceleration of 10^{20} eV protons is located between thick red lines H and D (the lower line, H, corresponds to the Hillas limit; the upper one, D, corresponds to the radiation-loss limit for diffusive acceleration).

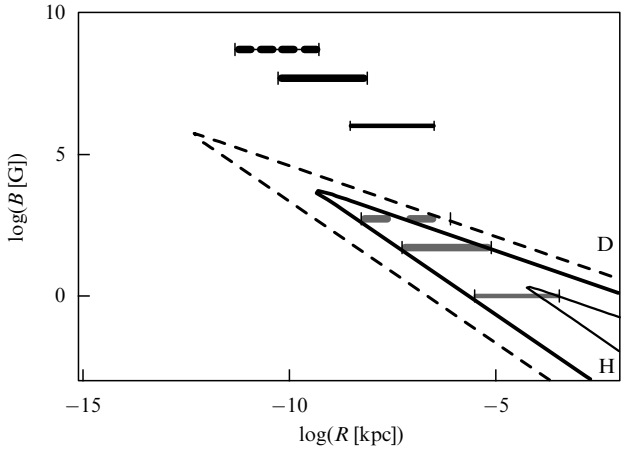

Figure 7. The size-field diagram for gamma-ray bursts. Horizontal lines represent estimates in Ref. [76], which assume a synchrotron origin for the prompt emission (dark grey) and the afterglow (light grey). The allowed region for acceleration of 10^{20} eV protons is located in between (the lower lines, H, correspond to the Hillas limit; the upper, D, correspond to the radiation-loss limit for diffusive acceleration). Dashed lines assume $\Gamma = 500$, thick lines assume $\Gamma = 50$, and thin lines assume $\Gamma = 1$.

magnetic fields in these extragalactic sites are measured indirectly. A summary of measurements is given in Fig. 6; a number of arguments in favor of higher (equipartition) fields in starburst galaxies were presented in Ref. [75], while continuity with the galactic measurements (see Fig. 6) may support lower (minimal-energy) estimates.

3.4 Gamma-ray bursts

Estimates of the magnetic field in gamma-ray bursts (GRBs) [76] assume that the origin of both prompt and afterglow emissions in a certain part of the spectrum is the synchrotron radiation of relativistic electrons. This assumption is supported by measurements of the afterglow spectra and light curves and by observation of the strongly polarized prompt emission (see Ref. [76] for a discussion and references). The values $B \sim 10^6$ G for $R \sim 10^{13}-10^{15}$ cm (prompt emission) and $B \sim 1$ G for $R \sim 10^{16}-10^{18}$ cm (afterglow) are given in Ref. [76] (we assume that the estimates correspond to the observer rest frame). Another, somewhat higher, field estimate can be obtained following Ref. [10] (see also Ref. [77]) from the total luminosity of a GRB, assuming that the magnetic field energy $\mathcal{E}_{\rm m}$ is a fraction $\epsilon_{\rm m} < 1$ of the radiation energy $\mathcal{E}_{\rm rad}$. However, this estimate depends strongly on the assumed beaming.

Within the scope of this paper, we can estimate the maximum energy $\mathcal{E}_{\rm max}$ of accelerated particles in the comoving frame following the equations in Section 2.4 for shock (diffusive) acceleration. But the GRB shells are ultrarelativistic ($\Gamma \sim 100$; see, e.g., Ref. [78]) and we have to multiply the comoving-frame $\mathcal{E}_{\rm max}$ by Γ to obtain the maximum rest-frame energy. The results are presented in Fig. 7, which, in the GRB case, is more instructive than the summary plots in Section 4. We note that at large Γ, the maximum energy may be limited by interactions with the thermal photon field (not taken into account in the present work) and *decreases* as Γ^{-1} for large Γ [10].

3.5 Galaxy clusters, superclusters, and voids

Information about cluster magnetic fields comes mostly from observations of their extended radio, and sometimes X-ray, emission. These observations are reviewed, inter alia, in Refs [28, 79, 80], where more references to original work can be found. Estimates based on equipartition (see, e.g., Refs [81, 82]), as well as those assuming Compton scattering on CMB photons, favor values $B \sim 0.1-1$ μG at megaparsec scales; Faraday rotation measurements (see Refs [83–85]) favor somewhat higher fields, $B \sim 1-5$ μG. Model-dependent numerical simulations remain the main source of information about magnetic fields at supercluster scales ($R \sim 100$ Mpc), especially in voids. Estimates range between $B \sim 10^{-11}$ G [86] and $B \sim 10^{-8}$ G [87].

4. Summary and discussion

Based on the data collected in Section 3 and on the limits on the maximum energy in Section 2.4, we here redraw the Hillas plot supplemented by radiation-loss constraints. Figures 8–10 give constraints for particular acceleration regimes, while Figs 11 and 12 represent our updated summary Hillas plots.

The weakest possible constraints (for inductive acceleration with curvature-dominated losses) are presented in Fig. 8. Constraints for inductive acceleration with synchrotron-dominated losses, applicable mostly to inner and outer jets of active galaxies, are given in Fig. 9, while constraints on the most general diffusive acceleration are presented in Fig. 10. Figure 11 represents our version of the Hillas plot with constraints for 10^{20} eV protons. Figure 12 is the same plot but for 10^{20} eV iron nuclei.

Constraints on neutron stars follow from Section 3.5; even for the least restrictive acceleration regime, they are not satisfied for UHE particles. In active galaxies, various acceleration regimes may operate. In the immediate vicinity of the central black hole (up to a few $R_{\rm S}$), the field configuration allows the inductive acceleration with curvature-dominated losses. These regions are indicated with 'BH' in Figs 8, 11, and 12; the parameters correspond to Eqns (14) and (11). The latter is an upper limit on the field, and we

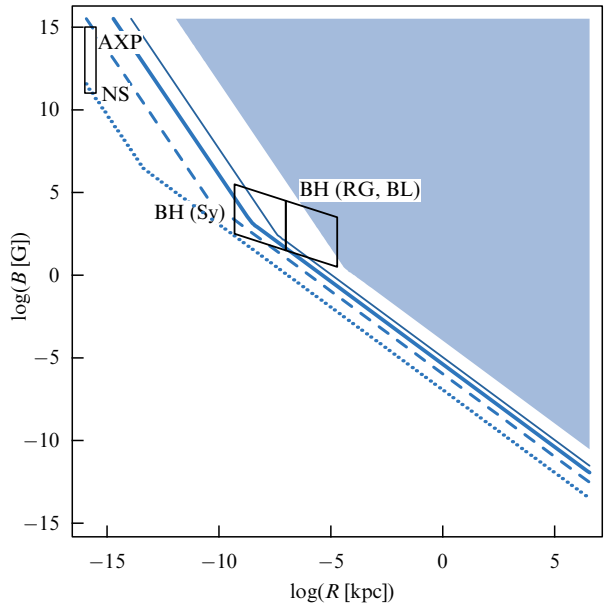

Figure 8. The size-field plot with constraints from geometry and radiation losses for the regime where losses are dominated by curvature radiation. These are minimum possible losses, and these constraints are therefore the weakest. Boxes denote parameter regions for objects in which conditions for this loss regime may be satisfied, that is, the immediate neighborhood of neutron stars (NS), anomalous X-ray pulsars and magnetars (AXP); and supermassive central black holes (BH) of active galactic nuclei, from low-power Seyfert galaxies (Sy) to powerful radio galaxies (RG) and blazars (BL). The shaded area corresponds to the parameter region where acceleration of protons to 10^{20} eV is possible. Lines show the lower bound of the allowed regions for 10^{19} eV protons (thin line), 10^{20} eV iron nuclei (thick line), 10^{18} eV protons (dashed line), and 10^{17} eV protons (dotted line). Right-hand parts of the lines represent the Hillas constraint, while left-hand (steeper) parts represent the radiation-loss constraint.

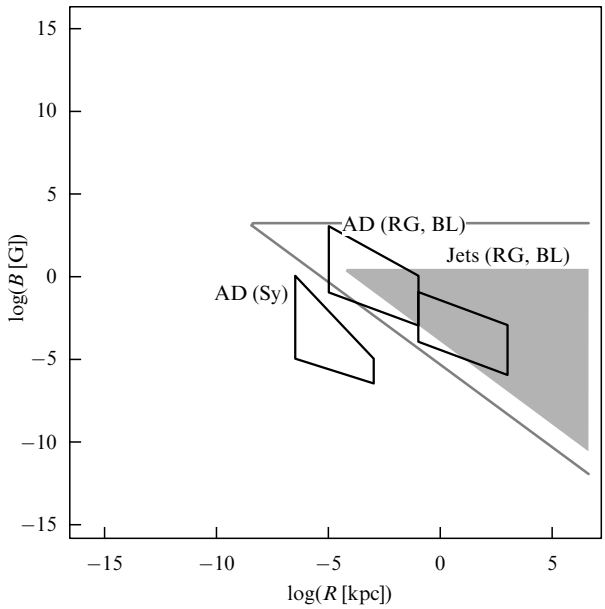

Figure 9. The size-field plot with constraints from geometry and radiation losses for the regime of one-shot acceleration with synchrotron-dominated losses. Boxes indicate parameter regions for objects in which conditions for this loss regime may be satisfied, that is, central parsecs (AD) of active galaxies (low-power Seyfert galaxies (Sy) and powerful radio galaxies (RG) and blazars (BL)) and relativistic jets of powerful active galaxies. The shaded area corresponds to the parameter region where acceleration of protons to 10^{20} eV is possible. The line bounds the allowed regions for 10^{20} eV iron nuclei. Lower lines represent the Hillas constraint, while upper (horizontal) lines represent the radiation-loss constraint. All quantities are given in the comoving frame, and therefore the maximum energy for jets must be multiplied by the bulk Lorentz factor of the jet, which can be as large as ~ 10 for leptonic jets and ~ 100 for hadronic jets [10].

therefore extend the boxes two orders of magnitude lower in B (cf. Fig. 2). Beyond the range of a few R_S, the $\mathbf{E} \| \mathbf{B}$ field structure no longer holds, but coherent fields may still be present in inner jets. For these central parsecs of AGN (indicated with 'AD' in Figs 9–12), we use the field estimates from Fig. 1. For the extended parts of active galaxies (jets, jet knots, hot spots, and lobes), we use field estimates summarized in Figs 4 and 5. The summary boxes for starburst galaxies include both equipartition and minimum-energy estimates (Fig. 6). For GRB, the summary plots present synchrotron-based estimates for both inner and outer shocks (see Fig. 7 for a more instructive plot). Field estimates for clusters, superclusters, and voids follow Section 3.5.

The constraints discussed here and expressed in terms of the Hillas plot are necessary, but they should be supplemented by other limits (listed at the beginning of Section 2). We note that in estimating the maximum attainable energy, important constraints are imposed by the interactions of accelerated particles with ambient photons. In particular, interaction with the cosmic microwave background is important for large sources, $R \gtrsim 1$ Mpc (lobes of radio galaxies, clusters, and voids), while interaction with the internal source radiation field is important for ultraluminuous sources (GRB and AGN). These constraints, considered elsewhere, further restrict the number of potential UHECR accelerators.[3] For a diffusive shock acceleration, these constraints have been studied, in particular in Ref. [9].

The maximum energy for supermassive black holes is readily expressed in terms of a single parameter, the black hole mass M_{BH}. We used the upper limit on the magnetic field B_{BH} that is most likely one or two orders of magnitude higher than the actual values, and hence our estimate in Eqn (15) is robust. It depends weakly ($\sqrt{R/R_S}$) on the assumed size of the acceleration region.

While we tried to make all constraints as robust as possible, it is clear that they should be regarded as order-of-magnitude estimates (in fact, the typical precision of the magnetic-field determination is an order of magnitude) and, for individual unusual field configurations, can be quantitatively violated. An example of such a configuration is a linear accelerator with the curvature radius r of field lines exceeding the source size R; then R should be substituted by r in Eqn (9). The estimates should be used with care in those cases where the magnetic field changes violently within the accelerator (for instance, when particles are accelerated by magnetic reconnection). A more detailed modeling of acceleration and losses is required in these cases.

One of our most important conclusions is that low-power active galaxies (e.g., Seyfert galaxies) cannot accelerate protons to energies $\gtrsim 5 \times 10^{19}$ eV. Indeed, when the extended structures (jets and outflows) are present, the magnetic field there is far too weak to satisfy the Hillas condition (even for very rare relativistic jets); see Fig. 4. The same is true for accretion disks, where the field is nicely

[3] In certain cases, proton–gamma interactions, instead of pure dissipation, can significantly amplify the acceleration process [19].

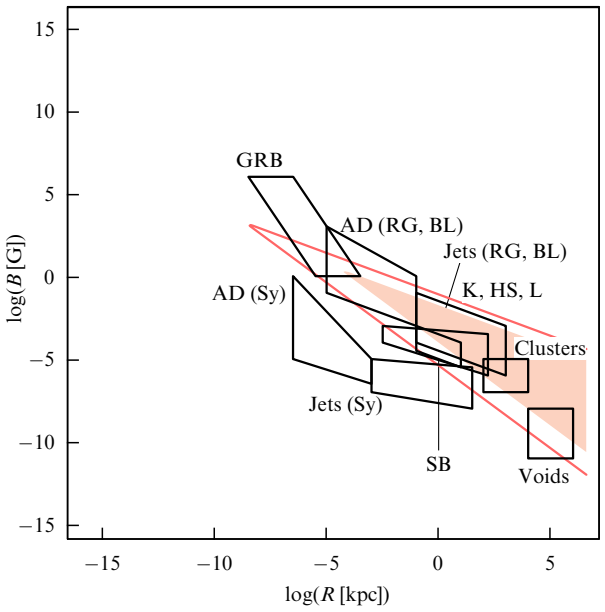

Figure 10. The size-field plot with constraints from geometry and radiation losses for the regime of diffusive acceleration with synchrotron-dominated losses. Boxes denote parameter regions for objects in which conditions for this loss regime may be satisfied, that is, central parsecs (AD) of active galaxies (low-power Seyfert galaxies (Sy) and powerful radio galaxies (RG) and blazars (BL)), relativistic jets, knots (K), hot spots (HS), and lobes (L) of powerful active galaxies (RG and BL); nonrelativistic jets of low-power galaxies (Sy); starburst galaxies; gamma-ray bursts (GRB); galaxy clusters and intercluster voids. The shaded area corresponds to the parameter region where acceleration of protons to 10^{20} eV is possible. The line bounds the allowed regions for 10^{20} eV iron nuclei. Lower lines represent the Hillas constraint, while upper lines represent the radiation-loss constraint. All quantities are given in the comoving frame, and therefore the maximum energy for jets and shells of GRBs must be multiplied by the bulk Lorentz factor, which can be as large as ~ 10 for leptonic jets and ~ 100 for hadronic jets and GRBs [10].

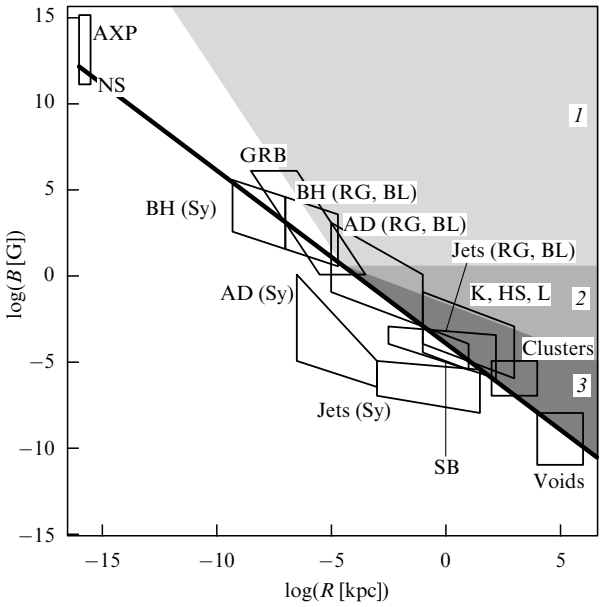

Figure 11. The Hillas plot with constraints from geometry and radiation losses for 10^{20} eV protons. The thick line represents the lower boundary of the area allowed by the Hillas criterion. Shaded areas are allowed by the radiation-loss constraints as well: light grey corresponds to one-shot acceleration in the curvature-dominated regime only; grey also allows one-shot acceleration in the synchrotron-dominated regime; dark grey allows both one-shot and diffusive (e.g., shock) acceleration. See captions to Figs 8, 9, and 10 for the notation of boxes corresponding to potential sources.

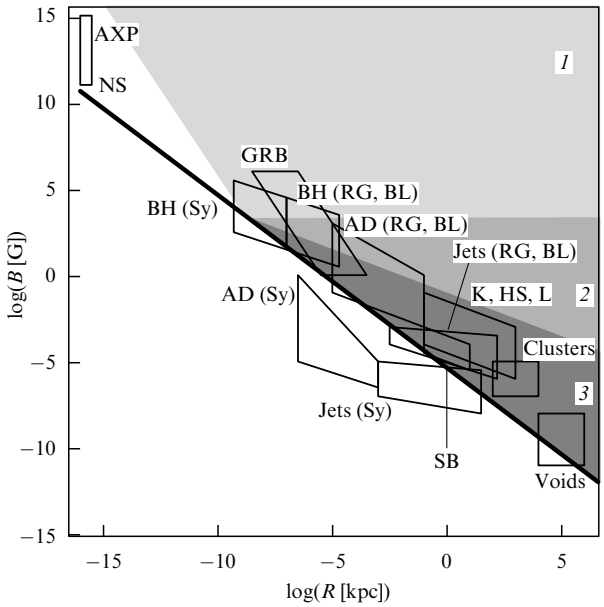

Figure 12. The same as Fig. 11 but for 10^{20} eV iron nuclei. The most important difference from Fig. 11 is that acceleration of iron nuclei to 10^{20} eV is possible (unlike for protons) in low-power active galaxies (e.g., Seyfert galaxies).

constrained from above by nonobservation of the Zeeman splitting in megamasers (Fig. 1). The most favorable conditions for acceleration correspond to the immediate vicinity (a few R_S) of the central black hole where the upper limit on the maximum energy is given by Eqn (15). Because $M_{BH} \lesssim (10^7 - 10^8) M_\odot$ for Seyfert galaxies, proton acceleration to $\sim 10^{20}$ eV is not allowed. However, these (and only these) central parts of Seyfert galaxies can, in principle, accelerate protons to $\sim 10^{18}$ eV and heavy nuclei to $\sim 10^{20}$ eV, if interactions with ambient photons are weak enough.

Although heavy nuclei are much less abundant than protons, Seyfert galaxies themselves are much more abundant, and hence typically closer to the observer than powerful radio galaxies and blazars, and their population can therefore contribute to the UHECR spectrum.

5. Conclusions

We reviewed constraints on astrophysical UHE accelerators and presented the Hillas plot supplemented with radiation-loss constraints and updated with recent astrophysical data. In contrast to previous studies, we emphasized that active galaxies span a large area on the plot, and only the most powerful ones (radio galaxies, quasars, and BL Lac type objects) are capable of accelerating protons to UHE. If UHECR particles are accelerated close to the supermassive black holes in AGNs, then the mechanism is most likely 'one-shot,' with energy losses dominated by the curvature radiation. Other potential UHE acceleration sites are jets, lobes, knots, and hot spots of *powerful* active galaxies, starburst galaxies, and shocks in galaxy clusters. Acceleration of particles in supercluster-scale shocks, gamma-ray bursts, and the inner part of AGNs is subject to additional constraints from $p\gamma$ interactions, which are not discussed here. Unlike protons, heavy nuclei can be accelerated to UHE in circumnuclear regions of low-power active galaxies. Because these galaxies are abundant, this contribution to the

UHECR flux may be important, leading to a mixed primary cosmic ray composition at the highest energies.

The authors are indebted to D Gorbunov, S Gureev, A M Hillas, V Lukash, A Neronov, S Popov, and D Semikoz for the interesting discussions. We acknowledge the use of online tools [53, 54]. This work was supported in part by the RFBR grants 07-02-00820 09-07-08388 (ST) and NS-1616.2008.2 (ST), and by FASI government contracts 02.740.11.0244 (ST) and 02.740.11.5092 (KP, ST).

6. Appendix. Derivation of electrodynamic results

A.1 Energy losses for the curvature radiation

We consider a particle moving along curved field lines (see [88]). The particle has a longitudinal velocity component ($\mathbf{v}_\parallel \parallel \mathbf{B}$) and a drift component ($\mathbf{v}_\mathrm{d} \perp \mathbf{B}$). This drift component induces the Lorentz force, which curves the particle trajectory toward the field lines. For a relativistic particle,

$$v_\mathrm{d} = \frac{{v_\parallel}^2 m}{qBr}\left(\frac{\mathcal{E}}{m}\right),$$

and hence the Lorentz force is

$$\mathbf{F}_\mathrm{L} = q\left[\mathbf{v}_\mathrm{d} \times \mathbf{B}\right],$$

$$F_\mathrm{L} = \frac{v_\parallel^2 m}{r}\left(\frac{\mathcal{E}}{m}\right).$$

The energy losses are in general determined by Eqn (5), which can be rewritten as

$$\frac{\mathrm{d}\mathcal{E}}{\mathrm{d}t} = \frac{2q^2}{3m^2(1-v^2)}\left[F^2 - (\mathbf{Fv})^2\right].$$

In the regime we consider, $\mathbf{Fv} = 0$, and therefore

$$\frac{\mathrm{d}\mathcal{E}}{\mathrm{d}t} = \frac{2q^2 v_\parallel^4}{3r^2}\left(\frac{\mathcal{E}}{m}\right)^4.$$

In the ultrarelativistic limit $v_\parallel \to c$, we obtain Eqn (9).

A.2 The maximum energy for diffusive acceleration

We consider a flow propagating through a magnetized medium. An accelerated particle gains energy by repeated scattering off the flow. After each scattering, the particle travels along the Larmor orbit, radiates, and decelerates according to Eqn (6); consequently,

$$\int_{\mathcal{E}_0}^{\mathcal{E}} \frac{\mathrm{d}\mathcal{E}}{\mathcal{E}^2} = -\frac{2q^4}{3m^4}\int_0^R B^2(x)\,\mathrm{d}x,$$

whence

$$\frac{1}{\mathcal{E}} = \frac{1}{\mathcal{E}_0} + \frac{2q^4}{3m^4}\int_0^R B^2(x)\,\mathrm{d}x.$$

The maximum energy $\mathcal{E} = \mathcal{E}_\mathrm{cr}$ is determined by letting $\mathcal{E}_0 \to \infty$,

$$\frac{1}{\mathcal{E}_\mathrm{cr}} = \frac{2q^4}{3m^4}\int_0^R B^2(x)\,\mathrm{d}x \simeq \frac{2q^4}{3m^4}\,B^2 R,$$

and we obtain Eqn (7).

References

1. Nagano M, Watson A A *Rev. Mod. Phys.* **72** 689 (2000)
2. Kachelriess M, arXiv:0801.4376
3. Greisen K *Phys. Rev. Lett.* **16** 748 (1966)
4. Zatsepin G T, Kuz'min V A *Pis'ma Zh. Eksp. Teor. Fiz.* **4** 114 (1966) [*JETP Lett.* **4** 78 (1966)]
5. Abbasi R U et al. (High Resolution Fly's Eye Collab.) *Phys. Rev. Lett.* **100** 101101 (2008)
6. Abraham J et al. (The Pierre Auger Collab.) *Phys. Rev. Lett.* **101** 061101 (2008); arXiv:0806.4302
7. Schlüter A, Biermann L *Z. Naturforsch. A* **5** 237 (1950)
8. Hillas A M *Annu. Rev. Astron. Astrophys.* **22** 425 (1984)
9. Protheroe R J *Astropart. Phys.* **21** 415 (2004)
10. Aharonian F A et al. *Phys. Rev. D* **66** 023005 (2002)
11. Medvedev M V *Phys. Rev. E* **67** 045401(R) (2003)
12. Gureev S, Troitsky S, arXiv:0808.0481
13. Kachelrieß M, Semikoz D V *Phys. Lett. B* **634** 143 (2006)
14. Landau L D, Lifshitz E M *Teoriya Polya* (The Classical Theory of Fields) (Moscow: Nauka, 1987) [Translated into English (Oxford: Pergamon Press, 1975)]
15. Longair M S *High-Energy Astrophysics*. Vol. 1 *Particles, Photons and Their Detection* (Cambridge: Cambridge Univ. Press, 1992)
16. Fermi E *Phys. Rev.* **75** 1169 (1949)
17. Blandford R, Eichler D *Phys. Rep.* **154** 1 (1987)
18. Rieger F M, Duffy P *Astrophys. J.* **617** 155 (2004)
19. Derishev E V et al. *Phys. Rev. D* **68** 043003 (2003)
20. Ostrowski M, arXiv:0801.1339
21. Schopper R, Birk G T, Lesch H *Astropart. Phys.* **17** 347 (2002)
22. Venkatesan A, Miller M C, Olinto A V *Astrophys. J.* **484** 323 (1997)
23. Neronov A, Semikoz D *New Astron. Rev.* **47** 693 (2003)
24. Neronov A, Tinyakov P, Tkachev I *Zh. Eksp. Teor. Fiz.* **127** 744 (2005) [*JETP* **100** 656 (2005)]
25. Neronov A, Semikoz D, Tkachev I, arXiv:0712.1737
26. Torres D F, Anchordoqui L A *Rep. Prog. Phys.* **67** 1663 (2004); astro-ph/0402371
27. Gorbunov D S, Troitsky S V *Astropart. Phys.* **23** 175 (2005)
28. Giovannini M *Int. J. Mod. Phys. D* **13** 391 (2004)
29. Vallée J P *New Astron. Rev.* **48** 763 (2004)
30. Mereghetti S *Astron. Astrophys. Rev.* **15** 225 (2008); arXiv:0804.0250
31. Bignami G F et al. *Nature* **423** 725 (2003)
32. Baring M G, Harding A K *Astrophys. Space Sci.* **308** 109 (2007)
33. Carroll B W, Ostlie D A *An Introduction to Modern Astrophysics* (San Francisco: Pearson/Addison-Wesley, 2007)
34. Zasov A V, Postnov K A *Obshchaya Astrofizika* (General Astrophysics) (Fryazino: Vek-2, 2006)
35. Véron-Cetty M P, Véron P *Astron. Astrophys. Rev.* **10** 81 (2000)
36. Fanaroff B L, Riley J M *Mon. Not. R. Astron. Soc.* **167** 31P (1974)
37. Vlemmings W H T, Bignall H E, Diamond P J *Astrophys. J.* **656** 198 (2007)
38. Modjaz M et al. *Astrophys. J.* **626** 104 (2005)
39. McCallum J N, Ellingsen S P, Lovell J E J *Mon. Not. R. Astron. Soc.* **376** 549 (2007)
40. Zavala R T, Taylor G B *Astrophys. J.* **566** L9 (2002)
41. Matveenko L I et al. *Pis'ma Astron. Zh.* **6** 77 (1980) [*Sov. Astron. Lett.* **6** 42 (1980)]
42. Artyukh V S, Chernikov P A *Astron. Zh.* **84** 896 (2007) [*Astron. Rep.* **51** 808 (2007)]
43. Tyul'bashev S A *Astron. Zh.* **82** 1081 (2005) [*Astron. Rep.* **49** 967 (2005)]
44. Chernikov P A et al. *Astron. Zh.* **83** 233 (2006) [*Astron. Rep.* **50** 202 (2006)]
45. Slish V I *Nature* **199** 682 (1963)
46. Zakharov A F et al. *Mon. Not. R. Astron. Soc.* **342** 1325 (2003)
47. Gnedin Yu M, Natsvlishvili T M, Piotrovich M Yu *Grav. Cosmol.* **11** 333 (2005)
48. Znajek R L *Mon. Not. R. Astron. Soc.* **185** 833 (1978)
49. Ghosh P, Abramowicz M A *Mon. Not. R. Astron. Soc.* **292** 887 (1997)
50. Shakura N I, Sunyaev R A *Astron. Astrophys.* **24** 337 (1973)

51. Novikov I D, Thorne K S, in *Black Holes* (*Les Houches, 23rd, 1972*) (Eds C DeWitt, B S DeWitt) (New York: Gordon and Breach, 1973) p. 343
52. Zhang W-M, Lu Y, Zhang S-N *Chin. J. Astron. Astrophys. Suppl.* **5** 347 (2005)
53. Paturel G et al. *Astron. Astrophys.* **412** 45 (2003); HyperLeda, http://leda.univ-lyon1.fr/
54. NASA/IPAC Extragalactic Database, http://nedwww.ipac.caltech.edu/
55. Harris D E, Krawczynski H *Annu. Rev. Astron. Astrophys.* **44** 463 (2006)
56. Gallimore J F et al. *Astron. J.* **132** 546 (2006)
57. Schurch N J, Roberts T P, Warwick R S *Mon. Not. R. Astron. Soc.* **335** 241 (2002)
58. Kataoka J et al. *Astrophys. J.* **641** 158 (2006)
59. Hardcastle M J et al. *Astrophys. J.* **670** L81 (2007)
60. Allen M G et al. *Astrophys. J.* **511** 686 (1999)
61. Laine S, Beck R *Astrophys. J.* **673** 128 (2008)
62. Burns J O, Feigelson E D, Schreier E J *Astrophys. J.* **273** 128 (1983)
63. Schwartz D A et al. *New Astron. Rev.* **47** 461 (2003)
64. Hardcastle M J et al. *Astrophys. J.* **612** 729 (2004)
65. Harris D E et al. *Astrophys. J* **699** 305 (2009); arXiv:0904.3925
66. Kataoka J, Stawarz Ł *Astrophys. J.* **622** 797 (2005)
67. Meisenheimer K et al. *Astron. Astrophys.* **219** 63 (1989)
68. Croston J H et al. *Astrophys. J.* **626** 733 (2005); astro-ph/0503203
69. Vlemmings W H T et al., astro-ph/0510452
70. Slysh V I, Migenes V *Mon. Not. R. Astron. Soc.* **369** 1497 (2006)
71. Vlemmings W H T *Astron. Astrophys.* **484** 773 (2008)
72. Sarma A P et al. *Astrophys. J.* **674** 295 (2008)
73. Curran R L, Chrysostomou A *Mon. Not. R. Astron. Soc.* **382** 699 (2007)
74. Anchordoqui L A, Romero G E, Combi J A *Phys. Rev. D* **60** 103001 (1999)
75. Thompson T A et al. *Astrophys. J.* **645** 186 (2006)
76. Piran T *AIP Conf. Proc.* **784** 164 (2005)
77. Lyutikov M, astro-ph/0409489
78. Piran T *Phys. Rep.* **314** 575 (1999)
79. Govoni F, Feretti L *Int. J. Mod. Phys. D* **13** 1549 (2004)
80. Ferrari C et al. *Space Sci. Rev.* **134** 93 (2008)
81. Beck R, Krause M *Astron. Nachr.* **326** 414 (2005)
82. Kronberg P P et al. *Astrophys. J.* **659** 267 (2007)
83. Clarke T E, Kronberg P P, Böhringer H *Astrophys. J.* **547** L111 (2001)
84. Taylor G B et al. *Mon. Not. R. Astron. Soc.* **368** 1500 (2006)
85. Govoni F et al. *Astron. Astrophys.* **460** 425 (2006)
86. Dolag K et al. *JCAP* (01) 009 (2005)
87. Sigl G, Miniati F, Enβlin T A *Nucl. Phys. B Proc. Suppl.* **136** 224 (2004)
88. Ginzburg V L, Syrovatskii S I *Proiskhozhdenie Kosmicheskikh Luchei* (The Origin of Cosmic Rays) (Moscow: Izd. AN SSSR, 1963) [Translated into English (New York: Gordon and Breach, 1969)]